[**Article ID**] 1003 - 6326(2002) 06 - 1218 - 06

Molecular dynamics of structural properties of molten CaO SiO₂ with varying composition

WU Yong quan(吴永全), HUANG Shir ping(黄世萍), YOU Jing lin(尤静林), JIANG Guor chang(蒋国昌)

(Shanghai Enhanced Laboratory of Ferro-Metallurgy, Shanghai University, Shanghai 200072, China)

[**Abstract**] Molecular dynamics simulations of the $x \operatorname{CaO}(1-x) \operatorname{SiO}_2$ melts (x varying with the composition of melt) were performed to achieve some structural information. It is found that the first peak positions of $\operatorname{Sr}\operatorname{Si}$, $\operatorname{Sr}\operatorname{O}$ and $\operatorname{O}\operatorname{O}$ partial radial distribution functions RDFs(3.165 Å 1.612 Å and 2.6 Å) agree very well with those of x-ray diffraction experiments. The discovered relation of coordinate number $N_{\operatorname{Sr}\operatorname{Si}}(r_0)$ with the molar ratio of CaO is linear and the slope is -0.056 17. The average bond lengths of $\operatorname{Sr}\operatorname{O}_b$ and $\operatorname{Sr}\operatorname{O}_{\operatorname{nb}}$ are 1.6275~ 1.630 Å and 1.595~ 1.60 Å respectively. Both distribution curves of the angles $\operatorname{O}\operatorname{Sr}\operatorname{O}$ and $\operatorname{Sr}\operatorname{O}\operatorname{Si}$ show one peak. For the distribution of angle $\operatorname{O}\operatorname{Sr}\operatorname{O}$ the positions of the peaks are just a little less than the typical tetrahedral angle 109.5°. And for angle $\operatorname{Sr}\operatorname{O}\operatorname{Si}$ the positions of peaks fluctuate in the range from 148° to 151°. At last, the distribution of five $\operatorname{Sr}\operatorname{O}$ tetrahedra was obtained and discussed.

[Key words] MD simulation, structural properties, CaO-SiO₂ melts

[CLC number] O 645; O 552.41; TF 01

[Document code] A

1 INTRODUCTION

The study of molten structure of CaO-SiO₂, which act as the basic factor influencing the physical and chemical properties of the silicate melts, has great importance in many fields, as metallurgy, mineralogy, geophysics, geology, and amorphous physics. For instance, the fluidity of metallurgical slag is mainly determined by the local structural units. In the latest decades, a number of techniques^[1~5] were devoted to gain the structural information of molten silicates. One of such methods is molecular dynamics simulation (MD). which has become a valuable tool for achieving insight into the structure of melts at the atomic level. The crucial factor in MD is the selection of a proper inter-atomic potential in order to represent the internal forces acting on the atoms^[1]. Then the simulation may go further to indicate the structural and chemicophysical properties of melts. As a generally accepted conception^[2~9], five Sr O tetrahedrons: Q_0 , Q_1 , Q_2 , Q_3 , and Q_4 corresponding respectively to none, one, two, three and four bridging oxygen in one tetrahedral unit are considered to be the basic local structural units. All of silicate melts are composed of these five tetrahedrons but in different proportion and intrinsic chemical potential.

In this paper, molecular dynamics simulations are performed to study the structural change, including RDFs $g_{ij}(r)$, coordination numbers $N_{ij}(r)$, bond angles of O-Si-O and Si-O-Si and so on, brought about by

increasing CaO fraction in the binary CaO-SiO2 melts.

2 SIMULATION METHOD

During the molecular dynamics simulations of CaO-SiO₂ melts, a type of pair potential of Born-Mayer-Higgins form was quoted^[4]:

 $u(r_{ij}) = q_i q_j / r_{ij} + B_{ij} \exp(-r_{ij} / Q_j)$ (1) where $u(r_{ij})$ is the interatomic pair potential and r_{ij} denotes the interatomic distance. The first term in the right hand side represents Coulomb repulsion interaction and the second term represents inter-core short-range repulsion interaction. The parameter values adopted for B_{ij} , and Q_{ij} have been discussed carefully elsewhere [4] and here only listed in the Table 1. The ionic valences q_i for Si, O, and Ca are +4, -2, and +2 respectively.

Table 1 Parameters for BMH potential $\rho_{ij}/$ Å B_{ii} / eV i-j 1.86602×10^{19} SrSi 0.025 SrO 0.1425 223 440. 54 Sr Ca 0.2226 1 362.401 O-Ca 0.3401 1 179. 225 Car Ca 0.4202 247.559 0.0 0.260 15 812. 842

In each simulation process, 630 atoms were included, and the initial construction is a random configuration that is most benefitting for the simulation of melts and

liquids. The model box lengths were changed slightly according to the proportion of CaO under the periodic boundary condition. The initial temperature is fixed at 6 000 K for 2 000 steps to mix the system completely. Then equilibration calculation is started and persisted for 5 000 steps to reach the required temperature of 2 000 K. Following equilibration calculation, the system is relaxed for 5 000 steps to discover the RDFs and correlation functions. So the total step number is 12 000, and the time step is 0.001 ps. As mentioned in previous section, the aim of this paper is to detect the structural change caused by increasing CaO fraction in the binary melt. So the numbers of Si, O, and Ca and the macrocompositions of melt would vary under the condition that the total atom numbers be fixed around 630. The atom numbers and the compositions are listed in Table 2.

3 RESULTS AND ANALYSES

3.1 RDFs and coordination numbers

Partial radial distribution functions (RDFs) $g_{ij}(r)$ is defined as the following equations for homogeneous and heterogeneous pairs:

$$g_{ii}(r) = \{ n_{ii}(r, r + \Delta r) / (4\pi r^{2} \cdot \Delta r) \} / \{ N_{i}(N_{i} - 1) / 2L^{3} \}$$

$$g_{ij}(r) = \{ n_{ij}(r, r + \Delta r) / (4\pi r^{2} \cdot \Delta r) \} / \{ N_{i}N_{i}/L^{3} \}$$
(2)

where $n_{ij}(r, r + \Delta r)$ is the number of ij atom pairs

with ij atom distance in the range $(r, r + \Delta r)$; N_i and N_j are the numbers of atom i and j in the unit box, respectively and L denotes the side length of the unit box. The simulation results are shown in Fig. 1. The positions of the first peaks of $g_{SrSi}(r)$, $g_{SrO}(r)$ and $g_{OO}(r)$ (3. 165 Å 1. 612 Å and 2. 6 Å), which represent the average distances of corresponding two atoms, agree well with the nearest neighboring distances observed by Waseda et al with x-ray diffraction [6] (3. 2 Å 1. 6 Å and 2. 66 Å) and that calculated by Belashchenko et al [8] (3. 26 Å 1. 63 Å and 2. 65 Å).

Table 2 Numbers of atoms and composition of melts

Sample	x (CaO) / % *	Ca	Si	0
I	30	70	163	396
II	35	83	155	393
III	40	97	145	387
IV	45	111	136	383
V	50	126	126	378
VI	55	141	116	373

^{* —}According to phase diagram $^{[6]}$, liquid region at 2 000 K is from 27% to 57% of CaO(mole fraction).

Fig. 1 also shows the results of coordination numbers from the equation as

$$N_{ij}(r) = 4\pi x_j \int_0^r g_{ij}(r') r'^2 dr'$$
 (4)

According to Fig. 1, the positions of the first

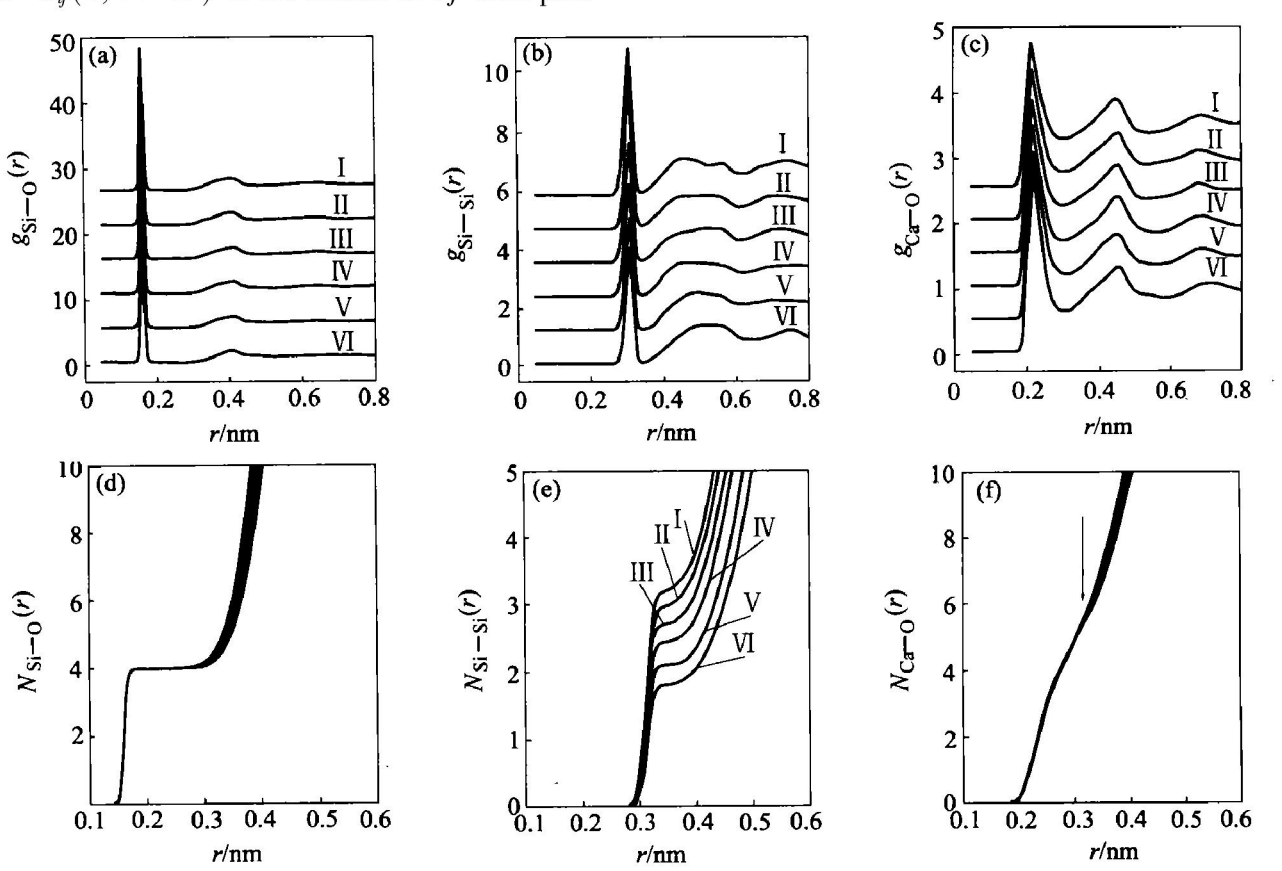


Fig. 1 Radial distribution function $g_{ij}(r)$ and coordination number $N_{ij}(r)$ for various compositions

 $g_{Si-O}(r)$ peaks are fixed at 1.612 Å and they are quite sharp peaks indeed, and almost no change to follow with the variation of CaO content in the melt. On the other hand, the peaks of $g_{CarO}(r)$ looks quite wide. They cover the range from smaller than 0.2 nm to larger than 0.3 nm. The coordinate number function $N_{Sr0}(r)$ displays an uniform platform fixed at 4 corresponding to xaxis value from 0. 17 nm to 0. 28 nm. From physical meaning of RDFs, in the radial range of 0.15~ 0.17 nm there are four oxygen around Si, which implies the typical SirO tetrahedron. But for $N_{\text{CarO}}(r_0)$ as the arrow shown in $N_{\text{Ca} O}(r)$ in Fig. 1(f), the y-axis value is about 5.65, a bit smaller than 6, which is universally accepted as the coordination number of network modifier^[10]. The facts mentioned above prove that the Si-O tetrahedra including some Ca²⁺ cations are the main local structural map. An instant snapshot of the Sample. (IV) is displayed in Fig. 2.

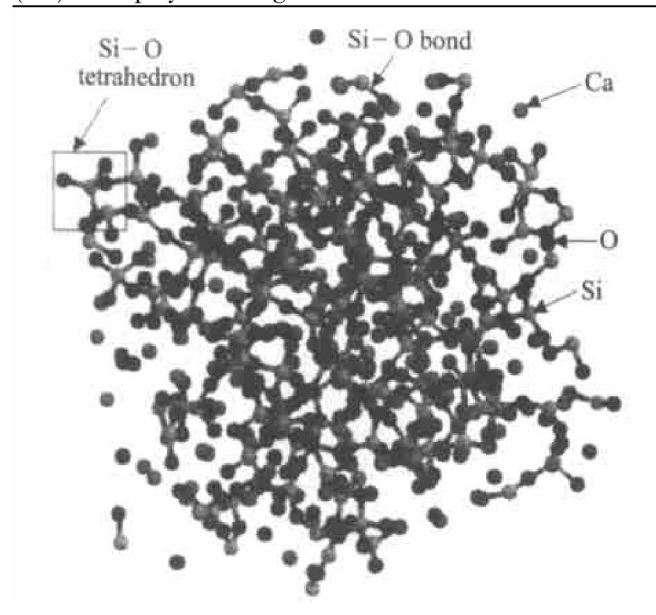


Fig. 2 Instant snapshot of Sample(IV)

The coordinate number $N_{\rm SrSi}(r_0)$, r_0 denotes the position of first mini of the curve $g_{\rm SrSi}(r)$, digitizes the polymerization degree of the melt. As shown in Fig. 3 it linearly varies pursuant to the content of CaO. Because ion Ca²⁺ plays as network modifier in the melt, the more the content of CaO, the lower the polymerization degree, and farther the distance between two Si⁴⁺. If microstructure of the melts goes by the stoichiometry for completely ideal state, which means that all of Si⁴⁺ in melts are network former and all Ca²⁺ are network modifier, the slope of the curve in Fig. 3 should be - 0.06. The value of the simulation result, - 0.056 17, is very close to the ideal value. So, conclusion can be reached that the structural distribution of calcium silicate melts follows stoichiometry comparatively firmly.

3. 2 Relative amount of bridging oxygen, norbridging oxygen and free oxygen

The relative amount of three different oxygen anions were calculated from 100 snapshots of equilibrated phases (one snapshot after an interval of 50 steps in the last 5 000 steps) and the cutoff distance is set to 2. 0 Å (within the distance, pair of Si and O can be regarded bonded). The distance was selected according to the platform of the $N_{\rm SirO}(r)$ curve, which corresponds to the first valley of $g_{\rm SirO}(r)$ (within the valley, $g_{\rm SirO}(r)$ = 0, which means that departed from any Si⁴⁺ there is no oxygen existed within the radial range from about 1.7 to 2. 6 Å).

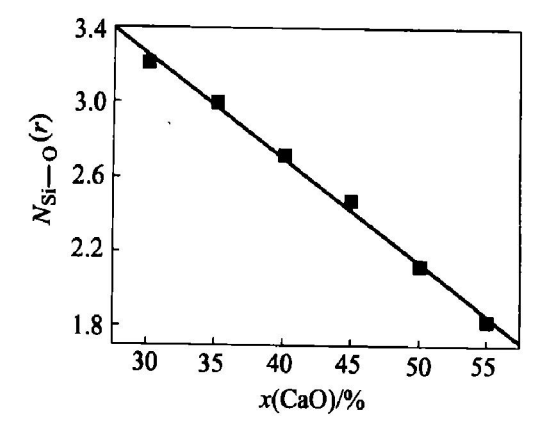


Fig. 3 Coordinate number $N_{\text{SrSi}}(r_0)$ varying with molar ratio of CaO

Fig. 4 exhibits the simulation results of the relative amount of three different oxygen anions and the Raman experimental results of TSIMAWALI^[5]. From comparison, the difference of simulation results and that of experiment is limited to 5%. Moreover, up to 5% free oxygen O^{2-} exists in the simulation results, but this concentration is undetectable in the experiment. If neglecting the existence of O^{2-} , the content of bridging oxygen $O_b(\ y_1)$ and non-bridging oxygen $O_{nb}(\ y_2)$ can be expressed as:

$$y_2 = 2x/(2-x)$$
 (5)

$$y_1 = (2 - 3x)/(2 - x)$$
 (6)

where x denotes the mole fraction of CaO in the melt. This is called ideal state as dash line shown in Fig. 4. Sprenger et al^[11] also proposed this relation. By means of the ESCA(Electron Spectroscopy for Chemical Analysis) technique, Jen et al^[12] and Bruckner et al^[5] measured the ratio of bridging oxygen to non-bridging oxygen in alkaline silicate melts and claimed that the ratio was around that indicating by Eqns. (5) and (6) just as shown in Fig. 5. From Fig. 5, not only the experimental data but also the simulated results fit very well with the solid line and support the ratio equation derived from Eqns. (5) and (6).

3. 3 Average bond length of Si O_b and Si O_{nb}

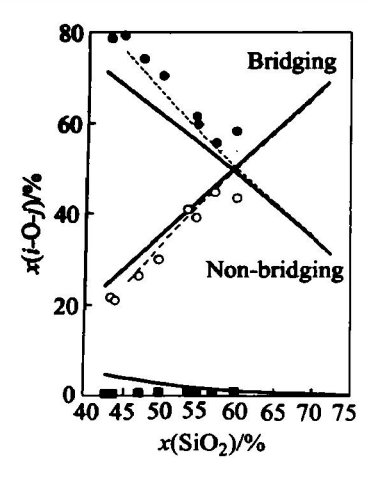


Fig. 4 Distribution of *i*-O-*j* Solid line—This work, at 2 000 K; dash line—Ideal state;

Plot —Experimented by Tsunawaki et al^[5] at 1 600 °C

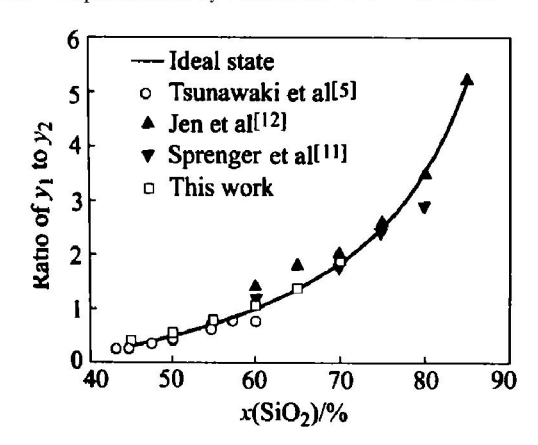


Fig. 5 Ratio of bridging oxygen to nor bridging oxygin

The simulation results of d_{SrO_b} and $d_{SrO_{nb}}$ (the average bond length of SrO_b and SrO_{nb}) are shown in Fig. 6. As expected, $d_{SrO_b} > d_{SrO_{nb}}$ due to that the attraction of Ca^{++} to O_{nb} is weaker than that of Si^{4+} . Fig. 7 showing the bond situation of magnesium silicate crystal was quoted from F. Liebau^[13] and interpretted the phenomenon in Fig. 6. It must be noted that the interatomic force has their effect on electron cloud distribution. Following the increase of CaO content, $d_{SrO_{nb}}$ becomes a bit longer from 1.594 Å to 1.601 Å gradually but the length d_{SrO_b} has almost no change. This means that the attraction of Si^{4+} or so called of the local polymeric cluster to O_{nb} is gradually weaken, because the local polymeric cluster was broken by Ca^{2+} and consequently became smaller.

3.4 The Distributions of angles O-Si-O and Si-O-Si

The distributions of bond angles O-Si-O and Si-O-Si are shown in Fig. 8 and Fig. 9, respectively, and were also attained from the selected 100 configurations. Fig. 8(b) is the magnify of the peaks in Fig. 8(a) after

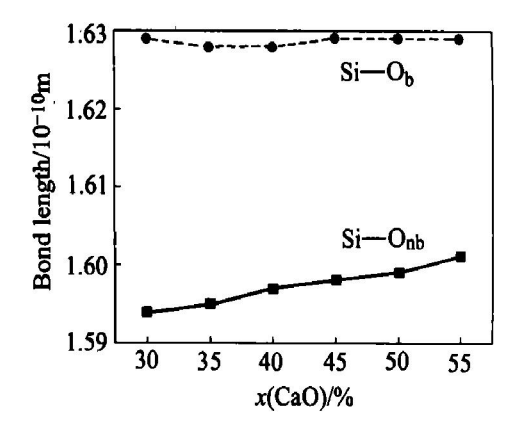


Fig. 6 Average bond length of SrO_{nb} and SrO_b

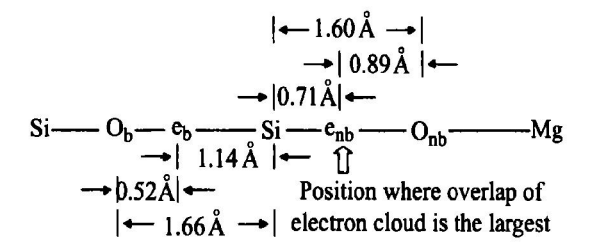


Fig. 7 The system of bonds of SrO_b-SrO_{nb}-Mg

smoothing transaction. It is clear that the peak of the distribution curves of O-Si-O angle is just beneath 109. 5° which is typical for tetrahedral crystal. And the positions of peaks shift to the right side along with the increase of CaO proportion. The distributions of Si-O-Si angles also exhibit peaks as shown in Fig. 9. Linking the tips of these peaks one can get a curve coincides with the fluctuation of $d_{\text{Si-O}_b}$ shown in Fig. 6. These are possible results, just as the relationship between $d_{\text{Si-O}_b}$ and angle Si-O-Si suggested by Liebau^[14] for solid silicate:

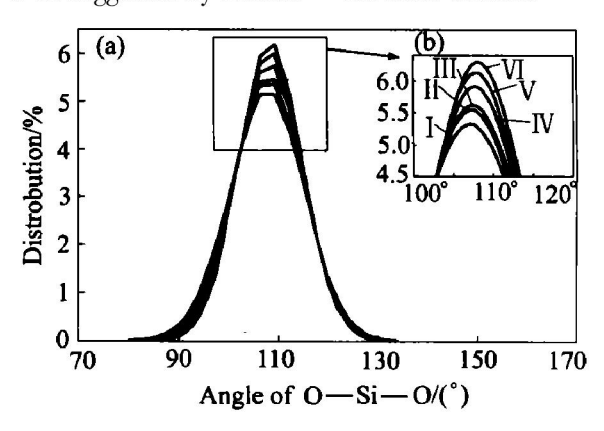


Fig. 8 The distribution of angle O- Si- O

3. 5 Tetrahedral unit content in melt of different composition

According to the results of high temperature Raman spectroscopy^[14], a concept is popularly accepted that various silicate are composed of SrO tetrahedrons. Gen-

erally, a single crystal of silicate only contains one kind of tetrahetron. But in molten or amorphous silicate, Mysen and McMillan^[2,3] concluded that there are always several kinds of tetrahedrons coexisted in silicate melts. In fact, many macro-properties of melts such like viscosity are mainly determined by the distribution of Si-O tetrahedrons. Totally, there are 5 kinds of tetrahedrons as shown in Fig. 10 which discovers the content variation of different tetrahedrons versus the increase of CaO molar fraction. By comparing the concentration in terms of Q_i of alkaline silicate glasses from²⁹Si MAS-NMR experiment^[15] and that of calcium silicate melts of this work shown in Fig. 10, similar trends of each tetrahedron with content of SiO₂ can be obtained.

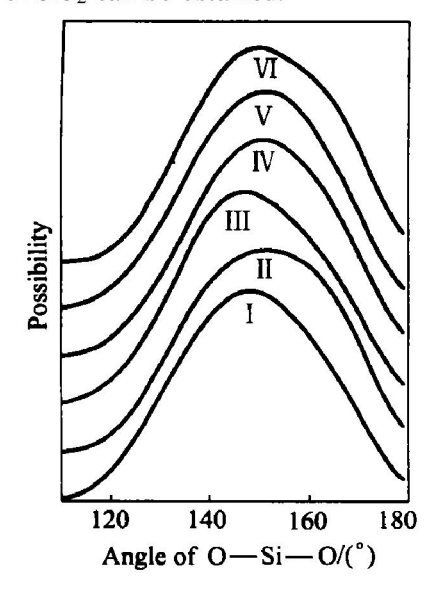


Fig. 9 Distribution of angle Si-O-Si

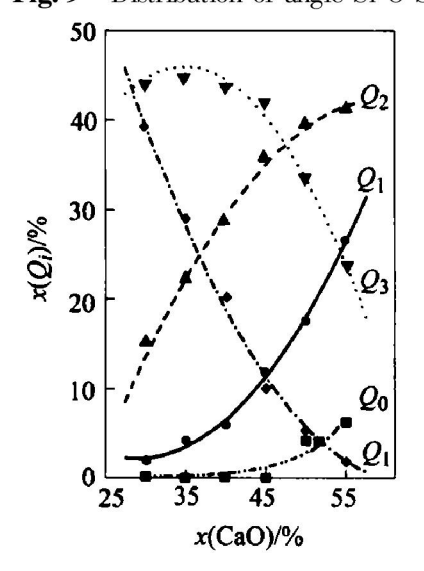


Fig. 10 Distribution of Q_i verus molar fraction of CaO

As shown in Fig. 10, the curve of Q_3 has a max corresponding to $x(\text{CaO}) \approx 35\%$ which is lightly higher than the content of crystalline silicate in Q_3 , x(CaO) = 33.3%. And in any calcium silicate melt there are ex-

actly several kinds of tetrahedrons coexisted. Integrating Fig. 10 with Fig. 4, one can conclude that the microstructure of calcium silicates with any composition are all composed with several kinds of $Q_{\rm i}$ units, cation Ca²⁺ and minute quantity of free oxygen ${\rm O}^{2-}$.

4 CONCLUSIONS

The structural information of CaO- SiO_2 melts with various compositions was achieved by means of molecular dynamics simulation (MD). The results agree with those of experiments very well. Based on this investigation, the follow conclusions can be claimed.

- 1) The characteristics of the peaks of $g_{SrO}(r)$ and $g_{CarO}(r)$, as well as $N_{SrO}(r)$ equal to 4 and $N_{CarO}(r)$ close to 6, indicating that the SrO tetrahedrons including some Ca²⁺ cations are the mainly local structure units.
- 2) $N_{\rm SrSi}(r_0)$, r_0 denotes the position of first mini of the curve $g_{\rm SrSi}(r)$, digitizes the polymerization degree of the melt. From the slope of the curve of $N_{\rm SrSi}(r_0)$ versus x (CaO), 0.056 17, conclusion can be reached that the structural distribution of calcium silicate melts follows stoichiometry comparatively firmly.
- 3) Up to 5% free $\mathrm{O^{2-}}$ can exist in the melts as this simulation pointed out. This concentration is undetectable in the experiment. If neglect the existence of these free $\mathrm{O^{2-}}$, then the content of bridging oxygen $\mathrm{O_{b}}$ and non-bridging oxygen $\mathrm{O_{nb}}$ can be expressed as

$$\frac{y_1}{y_2} = \frac{2 - 3x}{2x}$$

- 4) Following the increase of CaO content, $d_{SFO_{nb}}$ becomes a bit longer from 1.595 Åto 1.601 Ågradually. But d_{SFO_b} has almost no change. This is because that the polymers in melt become smaller when increasing CaO. So, the abstraction acted by polymer to its non-bridging oxygen becomes weaker.
- 5) The peak of the distribution curves of angle of O-Si-O is just beneath 109. 5° and angle of Si-O-Si is around 150°, and within the range from 110° to 180°.
- 6) The curve of Q_3 has a max corresponding to x (CaO) $\approx 35\%$ which is lightly higher than the content of crystalline silicate in Q_3 , x (CaO) = 33.3%. The total microstructural units should include several kinds of tetrahedrons, Ca²⁺ cations and minute quantity of free oxygen O^{2-} .

[REFERENCES]

[1] Huff N T, Demiralp E, Cagin T, et al. Factors affecting molecular dynamics simulated vitreous silica structures [J].

- J Norr Cryst Solids, 1999, 253: 133.
- [2] McMillan P. Structural studies of silicate glasses and melts applications and limitations of Raman spectroscopy[J]. Am Mineral, 1984, 69: 622.
- [3] Mysen B O, Virgo D, Seifert F A. The structure of silicate melts: Implications for chemical and physical properties of natural magma [J]. Rev of Geophy and Space Physics, 1982, 20: 353.
- [4] WU Yong quan, HOU Huar yu, CHEN Hui, et al. Coordination and bond properties of Al and Si ions in the system of Al₂O₅ SiO₂ melts[J]. Trans of Nonferrous Metals of China, 2001, 11(6): 965.
- [5] Tsunawaki Y. Analysis of CaO·SiO₂ and CaO·SiO₂ CaF₂ glasses by Raman spectroscopy [J]. J Norr Crystalline Solids, 1981, 44: 369.
- [6] Waseda Y, Toguri J M. Temperature dependence of structure of molten silicates M₂O multiplied by 2SiO₂(M equals Li, Na, and K) [J]. Trans ISIJ 1977, 17(10): 601.
- [7] Hwa L G, Hwang S L, Liu L C. Infrared and Raman spectra of calcium alumino silicate glasses [J]. J Norr Cryst Solids, 1998, 238: 193.
- [8] Belashchenko D K, Gopengauz I E, Grytsenko A B, et al. Computational study on structure of non-crystalline oxides 2MeO•SiO₂(Me= Mg, Ca, Sr, Ba, Fe)[J]. ISIJ International, 1992, 32: 990.

- [9] McMillan P F, Wolf G H, Poe P T. Vibrational spectroscopy of silicate liquids and glasses [J]. Chem Geology, 1992, 96: 351.
- [10] Xu Per chang. Raman Spectroscopy in Geosciences [M]. (in chinese). Xi an: Sanxi Science and Technology Press. 1996, 46.
- [11] Sprenger D, Bach B, Meisel W, et al. Discrete bond model(DBM) of sodium silicate glasses derived from XPS, Raman and NMR measurements[J]. J Norr Cryst Solids, 1993, 159: 187.
- [12] Jen J S, Kalinowski M R. An ESCA study of the bridging and norr bridging oxygen ratio in sodium silicate glass and the correlations to glass density and refractive index[J]. J Norr Crystalline Solids, 1989, 38/39: 21.
- [13] Liebau F. Structural Chemistry of Silicates: Structure, Bonding and Classification [M]. Beijing: Chinese Construction Industry Press, (in chinese). 1989.
- [14] YOU Jing-lin, JIANG Guor chang, XU Kuang di. High temperature raman spectra of sodium disilicate crystal, glass and its liquid[J]. J Norr Cryst Solids, 2001, 282: 125.
- [15] Maekawa H, Maekawa T, Kawamura K, et al. The structure groups of alkali silicate glasses determined from 29Si MAS-NMR[J]. J Norr Cryst Solids, 1991, 127: 53.

(Edited by LONG Huai-zhong)